Journal of Colloid and Interface Science 506 (2017) 308–318

Contents lists available at ScienceDirect

Journal of Colloid and Interface Science

journal homepage: www.elsevier.com/locate/jcis

Regular Article

Fouling behavior of silica nanoparticle-surfactant mixtures during constant flux dead-end ultrafiltration

Krzysztof W. Trzaskus, Sooi Li Lee, Wiebe M. de Vos, Antoine Kemperman *, Kitty Nijmeijer [1]

Membrane Science & Technology Cluster, MESA+ Institute for Nanotechnology, University of Twente, Faculty of Science and Technology, P.O. Box 217, 7500 AE, Enschede, The Netherlands

GRAPHICAL ABSTRACT

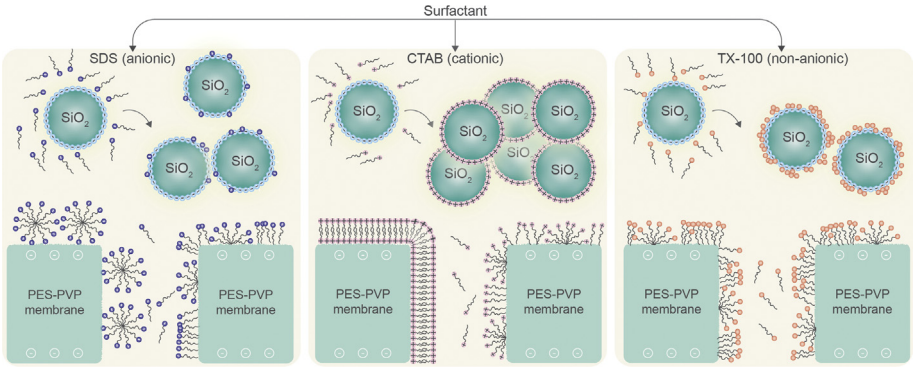

ARTICLE INFO

Article history:
Received 22 May 2017
Revised 13 July 2017
Accepted 14 July 2017
Available online 15 July 2017

Keywords:
Silica nanoparticle
Surfactants
Fouling
Ultrafiltration

ABSTRACT

The increasing use of engineered nanoparticles in customer products results in their accumulation in water sources. In this experimental study, we investigated the role of surfactant type (cationic, anionic and non-ionic) and concentration on fouling development, nanoparticle rejection and fouling irreversibility during dead-end ultrafiltration of model silica nanoparticles. Our work demonstrates that the type of surfactant influences the nanoparticle stability, which in turn is responsible for differences in fouling behavior of the nanoparticles. Moreover, the surfactant itself interacts with the PES-PVP membrane and contributes to the fouling as well. We have shown that anionic SDS (sodium dodecylsulfate) does not interact extensively with the negatively charged silica nanoparticles and does not change significantly the surface charge and size of these nanoparticles. Adsorption of the cationic CTAB (cetyltrimethylammonium bromide) onto the silica nanoparticles causes charge transition and nanoparticle aggregation, whereas non-ionic TX-100 (Triton X-100) neutralizes the surface charge of the nanoparticles but does not change significantly the nanoparticle size. The most severe fouling development was observed for the silica nanoparticle – TX-100 system, where nanoparticles in the filtration cake formed exhibited the lowest repulsive interactions. Rejection of the nanoparticles was also highest for the mixture containing silica nanoparticles and TX-100.

1. Introduction

The rapid growth of nanotechnology has resulted in multiple applications of engineered nanoparticles (NPs) [1]. The increasing production of such inevitably leads to their accumulation in the

* Corresponding author.
E-mail address: a.j.b.kemperman@utwente.nl (A. Kemperman).
[1] Current address: Membrane Materials and Processes, Eindhoven University of Technology, Department of Chemical Engineering and Chemistry, P.O. Box 513, 5600 MB Eindhoven, The Netherlands.

http://dx.doi.org/10.1016/j.jcis.2017.07.043
0021-9797/

aqueous environment after usage [2]. Over the last decades, membrane technology has been proven to be effective in the removal of colloidal particles such as proteins, natural organic matter (NOM) and inorganic particles [3–5] from water sources. Stability of the NPs plays a key role in their membrane filtration behavior using porous membranes[6–8]. Aggregation of nanoparticles in the bulk solution or at the membrane surface (due to concentration polarization) changes the size distribution of the solutes, and thus the rate of membrane pore blockage and porosity of the filtration cake formed [8–10]. Due to the high surface-area-to-volume ratio of nanoparticles, their stability is strongly related to their surface properties [11]. Often, to improve the stability of such dispersions various surface-active stabilizers (e.g. surfactants) are added [12–14]. The effectiveness of nanoparticle stabilization is determined by the type of the stabilizer, its affinity to the nanoparticles, and the concentration of both nanoparticles and stabilizers [11]. Adsorption of surfactants onto the nanoparticle surface may enhance electrostatic or steric repulsions between the nanoparticles, thereby reducing their tendency towards aggregation [15–17]. Furthermore, the presence of small non-adsorbing species (e.g. micelles) in the nanoparticle suspension leads to additional depletion stabilization [18]. On the other hand, adsorption of surfactants that only screens the surface charge of nanoparticles without providing an additional stabilization mechanism facilitates nanoparticle aggregation [19]. Furthermore, since adsorption of surfactants to NPs and micelle formation are concentration dependent [20–22], the concentration of the surfactant in the feed solution will play an important role in the nanoparticle stability as well.

Apart from nanoparticle stability, the presence of surface-active compounds will also change the interactions between the nanoparticles and the membrane. As a result, adsorption of the NPs onto the membrane surface is promoted or reduced, depending on the affinity between the surfactant and the membrane [23,24]. Despite the much smaller size of the surfactant molecules in comparison to the nanoparticles, they can form micelles that above the so-called critical micellar concentration (CMC) can be much larger than the NPs. Furthermore, surfactants may adsorb on the membrane or associate on the membrane surface as micelles or bi-layers above the so-called critical association concentration (CAC). All these effects will inevitably lead to more severe fouling when filtering suspensions containing nanoparticles and surfactants.

Literature on nanoparticle filtration in the presence of surfactants is limited. Up to our knowledge, work that focuses on a systematic comparison of the surfactant types (cationic, anionic, non-ionic) present in mixture of nanoparticles and role of the surfactant character on the nanoparticles filtration mechanism, is lacking. Therefore, the aim of this study is to understand the role of the surfactant type on nanoparticle filtration. Moreover, this publication intents to reveal implications that may occur during application of certain surfactant types during filtration of nanoparticles. Three types of industrially prominent surfactants are used: anionic sodium dodecylsulphate (SDS), cationic cetyltrimethylammonium bromide (CTAB), and non-ionic 2-[4-(2,4,4-trimethylpentan-2-yl)phenoxy]ethanol (Triton X-100). A detailed investigation of feed solution properties, combined with data from filtration experiments, allows determination of relevant mechanisms responsible for membrane fouling by nanoparticles in the presence of surfactants.

2. Materials and methods

2.1. Materials

Colloidal silica nanoparticles (Ludox TM-50) were used as model nanoparticles that were purchased as a 50% w/w suspension in water (Sigma Aldrich). Aqueous solutions of ACS grade NH_4-HCO_3-$(NH_4)_2CO_3$, HCl and NaOH (Sigma Aldrich) were used to adjust the pH and ionic strength of the solutions, respectively. Sodium dodecylsulfate (SDS), cetyltrimethylammonium bromide (CTAB) and Triton X-100 (TX-100) were purchased from Sigma-Aldrich. All solutions were prepared using ultrapure water (Milli-Q, resistivity >18.2 MΩ cm); all chemicals were used without further purification.

2.2. Membrane and membrane characterization

Commercially available inside-out polyethersulfone-polyvinyl pyrrolidone (PES-PVP) ultrafiltration (UF) membranes supplied by Pentair X-Flow BV (UFCLE type, MWCO 150 kDa) were used. UF filtration modules with a filtration area of 100 cm^2 were prepared by potting 10 hollow fiber membranes (inner diameter 0.8 mm, 40 cm long) in a PE tube (outer diameter 8 mm) with two-component polyurethane glue.

The membranes were characterized in terms of pure water permeability, inner surface charge and pore size distribution. The surface potential of the inner membrane was determined via streaming potential measurements using with a SurPASS electrokinetic analyzer (Anton Paar GmbH). In the experiments, we used 1 mM KCl as a background electrolyte solution; the pH was adjusted using aqueous 0.1 M NaOH and 0.1 M HCl solutions. The zeta potential was calculated according to the Fairbrother-Mastin equation [25]. The pore size distribution of the membranes was measured by permporometry. This technique is based on the controlled stepwise blocking of pores by condensation of a vapor, linked with the simultaneous measurement of the oxygen flux through the membrane [26]. Cyclohexane was used as the condensable vapor in our home made setup.

2.3. Characterization of nanoparticle – surfactant mixtures

The CMC values of cationic and anionic surfactants were determined using conductivity measurements of the solutions at 30 °C in the presence of 1 mM ammonium bicarbonate buffer. The CMC values were found as the intersection of the two slopes describing conductivity rise with surfactant concentration before and after micelle formation [27]. Conductivity was measured using a conductometer Cond 3210 (WTW GmbH, Germany). The CMC of the non-ionic TX-100 was determined using a force tensiometer K20 (Krüss GmbH, Germany) equipped with a Du Noüy ring. The CMC value was obtained by plotting the logarithm of the obtained surface tension versus the surfactant concentration. The CMC was estimated from the intersection of the linear regression line describing the decrease of the surface tension with the surfactant concentration below the CMC and the line describing a constant surface tension with increasing surfactant concentration above the CMC.

The hydrodynamic diameter of the nanoparticles in the mixture with surfactants was measured in batch mode using a DAWN-Heleos-8 modified at an angle of 108°, to which a dynamic light scattering (DLS) apparatus (NanoStar, Wyatt Technology Corporation, USA) was connected via a glass fiber cord. DLS measurements were carried out at a wavelength of 658 nm at 30 ± 1 °C. DLS data collection and analysis was performed using Astra® 6.1 software (Wyatt Technology Corporation, USA).

Electrophoretic mobility measurements of the silica nanoparticles were carried out via electrophoresis measurements using a Malvern ZetaSizer 3000Hsa (Malvern Instruments, United Kingdom) to obtain the zeta potential of the nanoparticles and their mixtures with surfactants. Both light scattering and zeta potential measurements were conducted using a 50 mg/L nanoparticle solution prepared in various concentrations of investigated surfactants

in 1 mM ammonium bicarbonate buffer solution. All experiments were repeated at least three times.

2.4. Filtration experiments

All feed solutions were prepared from a 1 mM ammonium bicarbonate buffer solution (Milli-Q water, pH 8) containing 50 mg/L of silica nanoparticles. The concentration of surfactants in the feed solutions was varied from 0.125 mM to 8 mM. The surfactant concentrations were chosen such to cover CMCs of all three surfactants in order to investigate the filtration behavior of silica nanoparticles below and above the CMC. The temperature of the feed solution was maintained at 30 °C by immersing the feed vessel in a temperature-controlled stirred water bath. Filtration experiments were started 24 h after the feed solution was prepared in dead-end filtration mode using an 'OSMO Inspector' filtration setup developed and automated by Convergence Industry B.V. (Enschede, The Netherlands). The schematic diagram of the filtration setup is given in Fig. 1.

The system contains a feed and a backwash pump (Liquiport® NF100, KNF, USA). By means of solenoid switching valves (Plasto-matic Valves, Inc. USA), the water from the backwash tank can be fed either to the feed or the permeate side of the membrane, enabling the integration of automatic pure water flux experiments. Two high-precision mass flow controllers (Cori-Flow™ model M15, Bronkhorst Cori-Tech, The Netherlands) are installed to measure and control the feed and backwash fluxes. Prior to filtration, the membranes were immersed in a 20 wt% ethanol solution for at least 24 h to remove conservation chemicals and to wet all the pores. After this, ultrapure water was filtered across the membrane modules at 2 bars for 10 min.

The OSMO software was programmed to perform single filtration-backwash experiments at a flux of 100 L/m h. The schematic description of the filtration-backwash experiment is shown in Fig. 2.

Firstly, at the beginning of each filtration experiment, the pure water permeability for each module was measured for 10 min at a flux of 100 L/m h (I). As a result of the applied potting procedure, the obtained permeabilities for the individual modules varied slightly due to small variations in the membrane surface area. Secondly, a feed solution containing silica nanoparticles and surfactants was introduced into the lumen of the fibers by a forward flush (II) that was carried out for 1 min. In the third step, the solenoid valve was switched to close the retentate outlet of the module and dead-end filtration (III) was started. The filtration was carried out under a flux of 100 L/m·h for one hour. After filtration, the shell side of the module was flushed with water (IV) for 1 min in order to remove the retentate present and to prepare the module for backwash (V), which was carried out for 30 min at 250 L/m h. Relatively long backwash times were applied to remove surfactant residues adsorbed to the membrane surface. After the backwash step, the lumen of the fibers was flushed (VI) with water for 1 min. In the last step, the permeability of the membrane (VII) was measured once again in order to calculate flux recovery. Each filtration experiment was repeated at least three times.

2.5. Data processing

Deposition of the nanoparticles on the membrane surface or inside the porous structure of the membrane leads to an increase of the filtration resistance, which can be calculated from Eq. (1):

$$R = \frac{\Delta P}{\eta \cdot J} \tag{1}$$

where R (1/m) is the hydraulic resistance, ΔP (Pa) is the transmembrane pressure, η (Pa·s) is the viscosity and J ($m^3/m^2 \cdot s$) is the flux.

The rejection of the solute by the membrane is defined by Eq. (2):

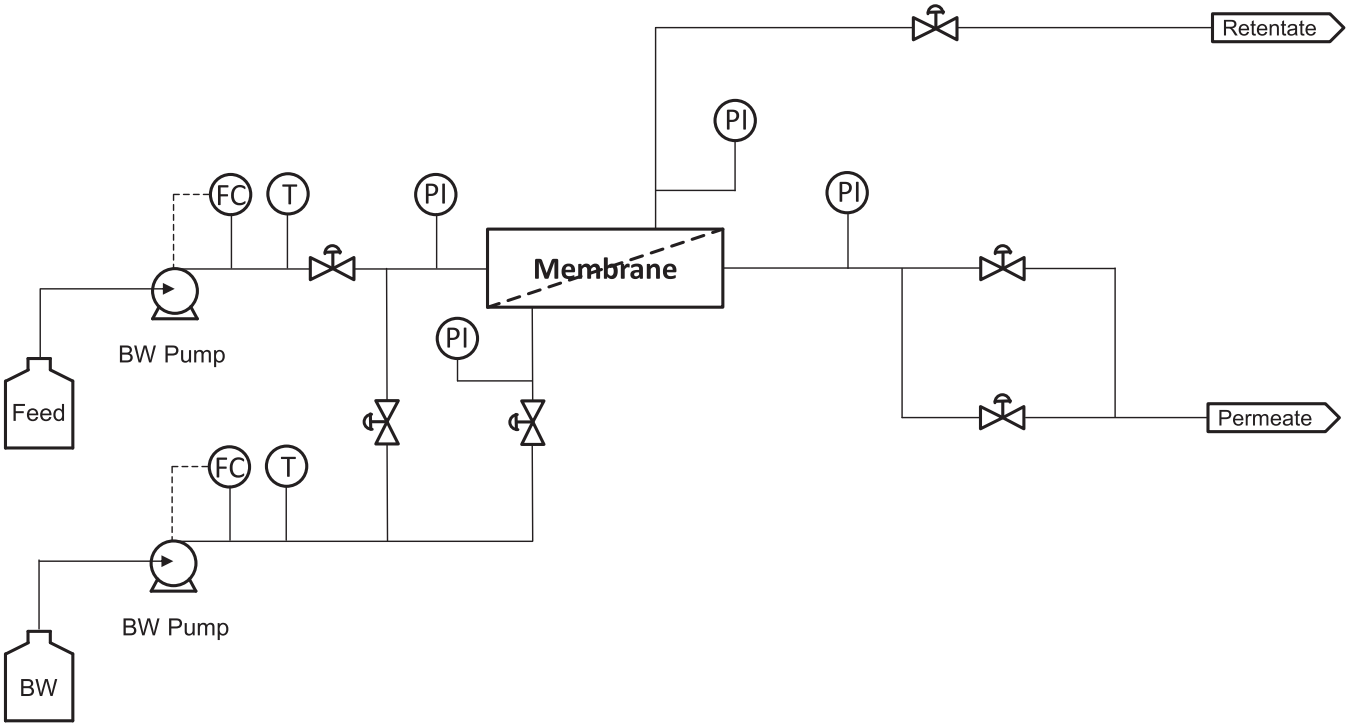

Fig. 1. Schematic diagram of the OSMO Inspector filtration setup. Feed and BW are feed and backwash water reservoirs, respectively. Two mass flow controllers (FC) control the feed and backwash flows. The pressure of the feed, the backwash, the permeate and the retentate is measured using pressure indicator (PI). The temperature (T) in the feed and downstream of the backwash pump is monitored as well.

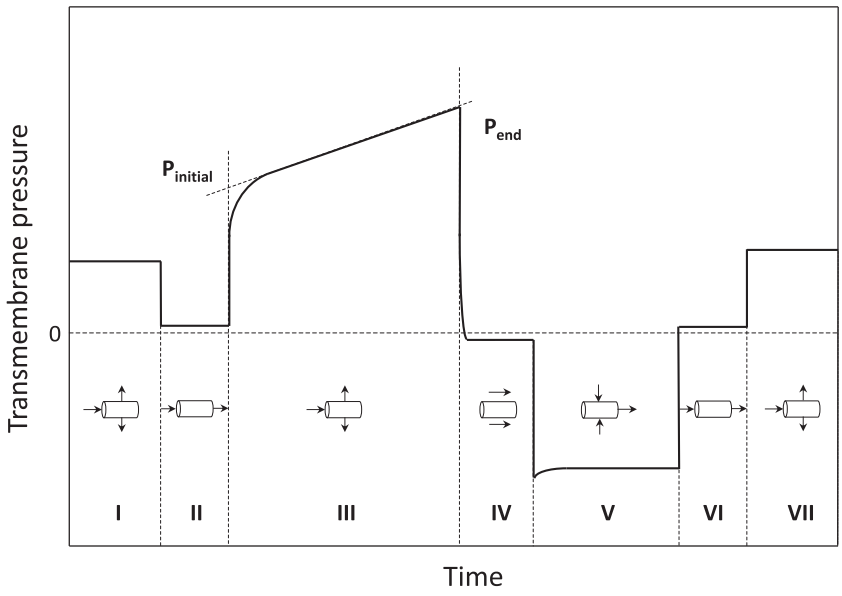

Fig. 2. Single filtration-backwash cycle (adapted from van de Ven et al. [28]). I – pure water permeation, II – forward flush with feed solution, III – filtration, IV – flush of the shell side, V – backwash, VI – forward flush with water, VII – pure water permeation.

Table 1
Properties of the applied membrane.

Membrane					
Type	Material	MWCO* [kDa]	Clean water permeability [L/m^2·h·bar]	Pore diameter [nm]	Zeta potential at pH 8 [mV]
Pentair X-Flow UFCLE	PES/PVP	150	$1 \pm 0.1 \cdot 10^3$	24 ± 5	−24.9 ± 3.4

* Manufacturer's data.

$$\sigma = 1 - \frac{C_p}{C_f} \quad (2)$$

where σ is the rejection (-), C_P is the concentration of the solute in the permeate sample (mg/L), and C_f is the concentration of the solute in the feed solution (mg/L). For a single filtration experiment 6 permeate samples were collected during the filtration. In order to evaluate the nanoparticle rejection, concentrations of nanoparticles in the feed and permeate samples were determined using Inductively Coupled Plasma Mass Spectrometry (ICP-MS; Thermo Fisher Xseries 2). Since rejections obtained were more or less constant during a single filtration experiment, we report average rejection values, which are obtained from averaging rejections calculated from 6 collected permeate samples in 3 repeated filtration runs (in total 18 permeate samples per rejection point).

The total fouling rate describes the fouling development as defined in the improved flux-step method developed by van der Marel et al. [29]. The fouling rate was calculated according to Eq. (3).

$$F_{tot} = \frac{P_{end} - P_{initial}}{\eta \cdot J \cdot \Delta t} \quad (3)$$

where R (1/m) is the hydraulic resistance, $P_{initial}$ (Pa) is the initial transmembrane pressure, P_{end} (Pa) is the final transmembrane pressure, η (Pa·s) is the viscosity, J (m^3/m^2·s) is the flux and Δt (s) is the filtration time.

The permeability recovery PR is used to describe irreversibility of the fouling and is defined as:

$$PR = \frac{R_m}{R_{mbw}} \quad (4)$$

where PR (-) is the permeability recovery, R_m (1/m) is the hydraulic resistance of the membrane before filtration (step I in Fig. 2) and R_{mbw} (1/m) is the hydraulic resistance of the membrane after the backwash step (step VII in Fig. 2).

3. Results and discussion

3.1. Membrane characteristics

The properties of the UF membrane used are listed in Table 1. The Molecular Weight Cut-Off (MWCO) reported by the manufacturer was 150 kDa. The experimentally determined pure water permeability measured was 1000 ± 100 L/m^2 h bar. According to the permporometry measurements, the mean pore diameter of this membrane was found to be 24 ± 5 nm. Streaming potential measurements showed that the inner surface of the membrane had a zeta potential of −24 ± 3 mV at pH 8.

3.2. Feed solution characteristics

The properties of the surfactants applied are listed in Table 2. The experimentally determined CMC the values are comparable to values reported in literature [27]. Above the CMC, surfactants form micelles, which varies in size for each surfactant type, as shown in Table 2. The Krafft temperature is the minimum temperature at which surfactants can form micelles. Since for CTAB this temperature is quite high (25 °C), we carried out all our experiments at 30 °C to ensure that all surfactants can form micelles.

Since surfactants are surface active molecules, they can adsorb onto nanoparticles and change their surface properties, such as charge. Correspondingly, this can lead to increased or reduced stability of the nanoparticles in a suspension, depending on whether the surfactants enhance or reduce repulsive interactions between the nanoparticles. The surface zeta potential and the

Table 2
Properties of the applied surfactants at 30 °C.

Surfactant	Type	M_w [g/mol]	CMC [mM]	Micelle diameter [nm]	Krafft temp. [°C]
SDS	Anionic	288	7.49	3.7 [30]	18 [31]
CTAB	Cationic	364	0.99	7 [32]	25 [33]
TX-100	Non-anionic	647	0.25	7.4 [34]	<0 [35]

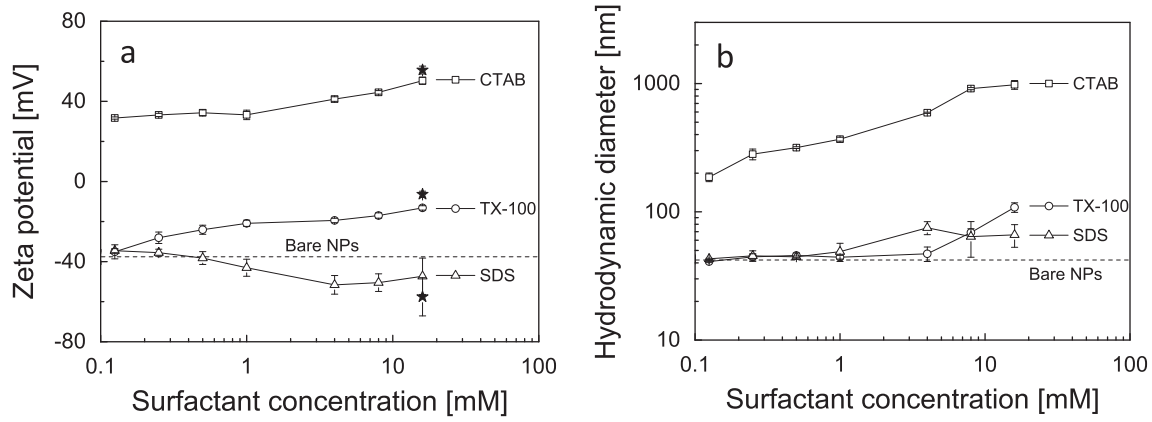

Fig. 3. Zeta potential (a) and hydrodynamic diameter (b) of silica nanoparticles as a function of the CTAB, TX-100 or SDS surfactant concentration at pH 8 at 30 °C. The stars represents pure surfactant suspension at 16 mM.

hydrodynamic diameter of the silica nanoparticles as a function of the surfactant concentration at pH 8 are shown in Fig. 3a and b, respectively. To take into account the behavior of the pure surfactants, zeta potential measurements were also conducted with pure surfactant suspensions at a concentration of 16 mM, which are represented as star symbols in Fig. 3a.

As Fig. 3a shows, the zeta potential of the silica nanoparticles becomes slightly more negative in the presence of the negatively charged SDS compared to bare silica without any added SDS. These results are rather surprising as both silica and SDS are negatively charged, and hence we would not expect any adsorption of SDS onto silica [36]. Nonetheless, our observations indicate that SDS could be adsorbed in small amounts onto the silica surface. Ahualli et al. [15] reported a similar effect in electrophoretic mobility measurements of silica NPs in SDS solutions ranging from 0.01 mM to 8 mM SDS. They observed an increase in the negative mobility and zeta potential and attributed the observation to a super charging effect that increased the effective charge of the silica nanoparticles (possible because only part of the interaction between silica and SDS is electrostatic) [15]. Another possible explanation for this observation could be the adsorption of small amounts of SDS onto the heterogeneities on the colloidal silica surface [17].

Fig.3b shows a slight increase of the hydrodynamic diameter of the nanoparticles with the SDS concentration. These findings suggest either a limited aggregation of the nanoparticles or the presence of some large impurities in SDS (the applied SDS was 90% pure). Nevertheless, we can conclude that addition of SDS to the nanoparticle suspension has only a little effect on both nanoparticle charge and size. In the case of CTAB-silica systems, an addition of positively charged CTAB modifies the silica surface from negative to positive, implying strong adsorption of CTAB onto the nanoparticle surface. This process has been extensively studied using various techniques [37–39]. CTAB can adsorb onto the silica surface due to (i) surface charge neutralization, (ii) hydrophobic interaction by the long hydrocarbon tail, or (iii) a combined effect of these two mechanisms [39,40]. In this study, however, we also observe that with the addition of CTAB to the silica nanoparticle suspension, the hydrodynamic diameter increases significantly, indicating the formation of larger aggregates (Fig. 3b). As such, we can conclude that aggregation occurs due to the adsorption of CTAB on the silica surface. During the adsorption of CTAB molecules onto silica surface, a negative charge of the nanoparticles is neutralized and thus repulsive interactions between nanoparticles vanish allowing aggregation. Further addition of CTAB causes nanoparticle charge transition to positive. The kinetic of this transition from positive to negative charge of the silica nanoparticles is mainly responsible for nanoparticle aggregation and size of the aggregates.

As shown in Fig. 3a, with increasing TX-100 concentration, the zeta potential becomes less negative. For pure TX-100 (being a non-ionic surfactant), the measured zeta potential at 16 mM was about -6.4 ± 1.6 mV, which is much less negative than the value obtained for bare silica nanoparticles. This is an indication of surfactant adsorption and shielding of the nanoparticle charge by TX-100. The work of Levitz et al. [41], Giordano-Palmino et al. [22] and Alexeev et al. [16], showed that TX-100 can adsorb effectively onto the colloidal silica surface as individual molecules at low concentrations via hydrogen bonding, followed by the formation of micelles on the nanoparticle surface through association at higher concentrations. Furthermore, similarly to the SDS case, at 8 mM of TX-100, a slight increment in the hydrodynamic diameter is observed, probably due to nanoparticle aggregation due to reduced repulsive interactions between the nanoparticles upon adsorption of the surfactant.

These results show that the type of the surfactant has a significant effect on the nanoparticle charge and size in the suspension. SDS interacts only slightly with the silica nanoparticles and no significant charge or size change is observed. CTAB reverses the nanoparticles charge and causes their aggregation. In the case of the non-ionic surfactant TX-100, the nanoparticle charge is reduced but nanoparticle aggregation is not significant. These insights are essential to explain filtration behavior of nanoparticles-surfactant mixtures.

3.3. Filtration experiments

3.3.1. Filtration of pure surfactant and bare nanoparticles

The resistance development during constant flux filtration of the feed solutions containing bare silica nanoparticles (50 mg/L) or pure surfactants (8 mM) is shown in Fig. 4a.

In comparison to the surfactants (of which the concentration was 2.31 g/L, 2.92 g/L, and 5.18 g/L for SDS, CTAB and TX-100, respectively), the applied concentration of nanoparticles was considerably lower (50 mg/L). Therefore, the lowest filtration resistance was obtained for the filtration of bare silica nanoparticles. Due to their high stability, the nanoparticle deposit is porous and permeable, and thus the resistance increases only gradually with the permeate volume, as shown in Fig. 4a. The thickness of the filtration cake at the end of the filtration was estimated to be about 3.1 μm taking into account the mass of deposited nanoparticles, assuming a hexagonal packing in the filtration cake and a uniform distribution along the module length.

As shown in Fig. 4a, pure surfactants at a concentration of 8 mM contribute significantly to the membrane fouling. The highest resistance was generated during the filtration of the ionic surfactants – SDS and CTAB. A significantly lower resistance was observed for the non-ionic TX-100. For all three surfactants, hydrophobic interactions between the hydrophobic tail of the surfactant and the hydrophobic PES polymer molecules in the membrane are expected to be responsible for surfactant adsorption onto the membrane surface [42], as schematically shown in Fig. 5. Furthermore, for anionic SDS, Prasad et al. [23] reported the presence of attractive interactions between the negatively charged SDS and the polarizable pyrrolidone group of PVP in the membrane, which would result in the formation of micelle-like aggregates on the membrane surface by association (Fig. 5). For

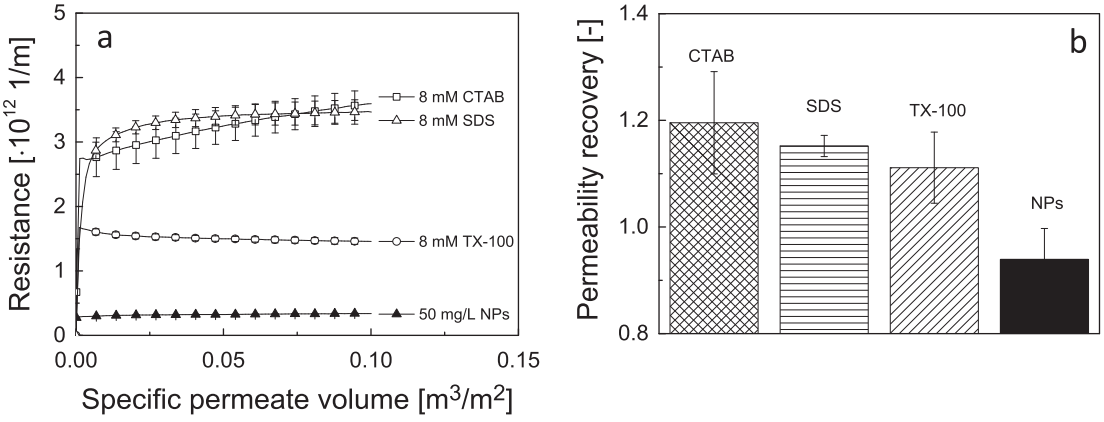

Fig. 4. Resistance (a) and permeability recovery (b) during filtration of pure surfactants and bare silica nanoparticles.

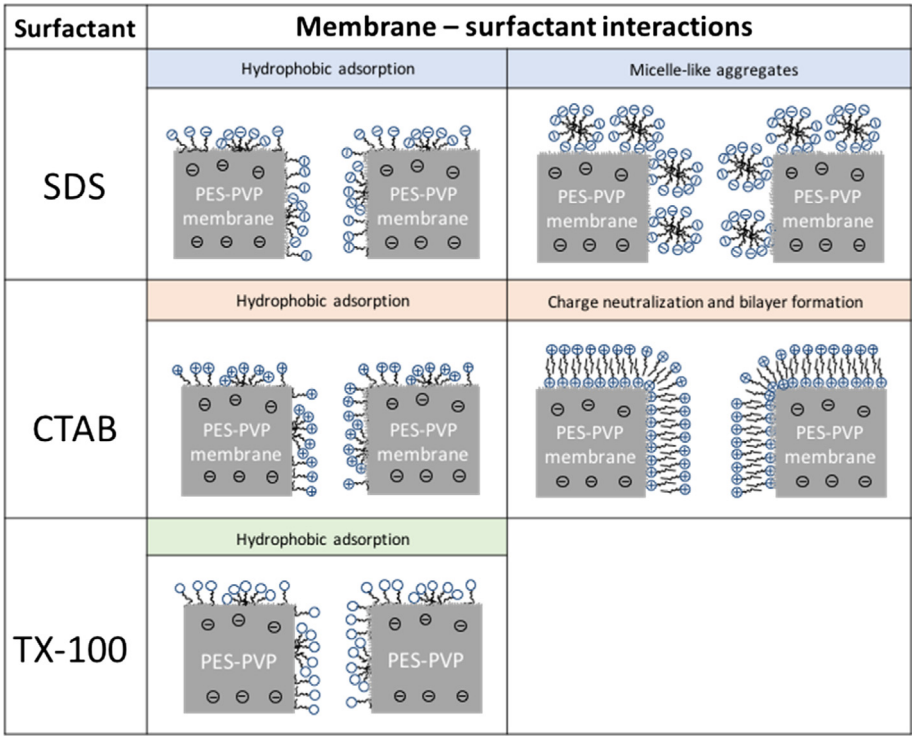

Fig. 5. Schematic representation of a possible interactions between a PES-PVP membrane and SDS (negative), CTAB (positive) and TX-100 (neutral) surfactants.

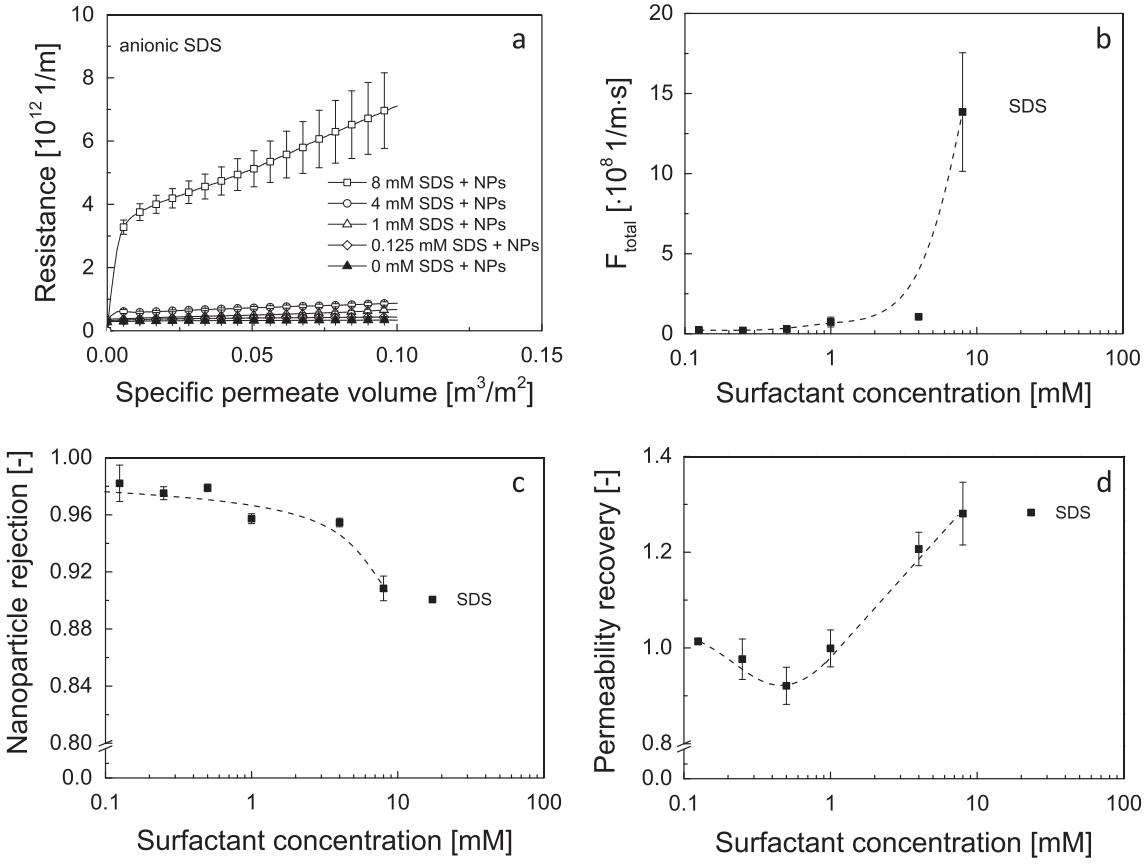

Fig. 6. (a) Resistance development as a function of permeate volume, (b) fouling rate, (c) rejection of nanoparticles and (d) permeability recovery as a function of surfactant concentration during constant flux dead-end filtration of 50 mg/L silica nanoparticles with anionic SDS at 30 °C. Dashed lines are drawn to guide the eye.

cationic CTAB, electrostatic attractions between the positively charged head group of the CTAB molecule and the negatively charged membrane can be considered as an additional adsorption mechanism (Fig. 5). All these adsorption mechanisms contribute to surfactant deposition onto the membrane surface and inside the pores, enhancing the hydraulic resistance. For all three surfactants, subsequent stabilization of the resistance (Fig. 4a) can be related to saturation of the membrane with the surfactant. The maximum surfactant adsorption capacity of the membrane is reached and transport of surfactant through the membrane pores becomes undisturbed again. As a result, we do not observe any measurable surfactant rejection. This is expected when we take into account the size difference between the membrane pores (Table 1) and the size of single surfactant molecules or even the micelles formed by the surfactants (Table 2).

As Fig. 4b shows, for all three pure surfactants the permeability recovery is higher than 1 (PR > 1). These results clearly indicate that the surfactants contribute to the enhancement of the pure water permeability regardless of their adsorption during the filtration. We attribute this effect to improved wetting of the fibers by the surfactant [43,44]. This clearly shows that the surfactants do not only influence the properties of the nanoparticles but also the membrane characteristics. In contrast to the results obtained for surfactants, the permeability recovery during the filtration of bare silica nanoparticles is lower than 1 (PR < 1, see Fig. 4b) indicating irreversible fouling.

3.3.2. Fouling development of nanoparticles in the presence of anionic SDS

We also investigated the combined role of the surfactant type and the concentration on fouling development during dead-end filtration of silica nanoparticles. Fig. 6 summarizes the filtration results obtained during filtration of silica nanoparticles with various concentrations of the anionic surfactant SDS.

Fig. 6a shows that for all SDS concentrations investigated (0.125 mM–8 mM), an increase of the surfactant concentration in the feed solution results in a higher hydraulic resistance, although this effect is less pronounced for lower concentrations. These findings are opposite to previous studies, which reported that addition of surfactant at low concentrations can result in reduced fouling. Singh and Song [18] investigated the influence of the SDS concentration on fouling development during cross-flow filtration. They postulated that addition of SDS in concentrations below 0.3 mM allows the formation of a more loosely packed cake on the surface of UF membrane. Hence, a lower fouling rate was obtained. However, in our case even for the lowest SDS concentration (0.125 mM), this effect was not observed. We relate this difference in fouling behavior of silica nanoparticles to the filtration mode at which the experiments were carried out (cross-flow in the case of Singh and Song and dead-end in this work) and limited interactions between nanoparticles and surfactants. The formation of a more porous cake layer in the presence of SDS, as proposed by Singh and Song, could only occur if the electrostatic repulsions between the nanoparticles are enhanced. However, this is not the case for our feed solution since the zeta potential measured reduces only slightly with increasing SDS concentration. Therefore, the synergic contribution of the SDS molecules to fouling development dominates the effect of the increased surface charge of the nanoparticles. As a result, the filtration resistance slightly increases with SDS concentration, despite the slightly higher repulsive interactions between the nanoparticles (Fig. 3a). Interestingly, below 8 mM SDS the filtration resistance is on a significantly lower level

(the maximum obtained resistance at 4 mM was $8.7 \cdot 10^{11}$ 1/m) than the resistance obtained at 8 mM of SDS (maximum obtained resistance $7.1 \cdot 10^{12}$ 1/m). This difference in the fouling development is clearly illustrated in Fig. 6b, where the fouling rate is plotted as a function of the surfactant concentration. The obtained fouling rate rises only marginally with SDS concentrations below 8 mM, but it significantly increases at 8 mM. Such behavior can originate from the fact that at 8 mM, SDS forms micelles (CMC of SDS for our system was in approx. 7.5 mM, see Table 2). This is in contrast to lower concentrations. At 8 mM, these micelles can also contribute to the filtration resistance. Consequently, due to the small effect of SDS on nanoparticle stability, there is only a limited contribution of SDS to fouling development below the CMC of SDS. However, above the CMC the micelles formed contribute strongly to the filtration resistance which can be related to the formation of a gel layer that is expected to have a significantly higher resistance than a cake layer [45,46].

The rejection of silica nanoparticles during their filtration in the presence of SDS as a function of the surfactant concentration is given in Fig. 6c. The rejection of bare silica nanoparticles during the complete filtration course was approx. 98 ± 1%. Such a high rejection was expected since the average pore size (see Table 1) is approximately the average size of the silica nanoparticle, as reported elsewhere [47]. Retention of nanoparticles is not only caused by size exclusion of the nanoparticles, but also by adsorption of the nanoparticles onto the membrane surface [48]. These two effects result in a more effective pore blockage and thus a more effective nanoparticle retention by the formation of a cake layer on the membrane surface, acting as an additional barrier for silica nanoparticles.

Addition of the SDS to the feed solution contributes to a noticeable reduction of the nanoparticle rejection, as shown Fig. 6c. Lower SDS concentrations (0.125–0.5 mM) do not change the nanoparticle rejection significantly. However, further increase of the SDS concentration gradually reduces the nanoparticle rejection to approx. 91% at 8 mM of SDS. This decrease in rejection can be related to the reduced interactions between the nanoparticles and the membrane after adsorption of SDS to the membrane and to the nanoparticles. Nanoparticle adsorption onto the membrane is reduced since the adsorption sites are already occupied by SDS. Consequently, the nanoparticles will block the pores less effectively. Moreover, slightly enhanced repulsive interactions between the nanoparticles in the filtration cake formed and a less ordered structure of the filtration cake in the presence of SDS micelles both cause the cake layer to be more open [49]. This results in an easier diffusion of the nanoparticles through the filtration cake and consequently in a lower rejection.

As described in Section 2.4, a pure water permeability check was carried out before filtration with the nanoparticle suspension and after the backwash procedure. The purpose of this was to ascertain the effect of the surfactant concentration and type on the extent of irreversible fouling. If nanoparticles irreversibly deposit on the membrane surface and irreversible fouling occurs, we expect a PR of <1. As shown in Fig. 4b, filtration of the pure surfactants leads to PR > 1. We relate this to better wetting of the membrane in the presence of surfactants, which makes the surface of the membrane more hydrophilic. Fig. 6d shows the permeability recovery as a function of the SDS concentration. At lower SDS concentrations (0.125–mM) the permeability recovery is approx. 1. However, it increases to values of 1.21 ± 0.07 and 1.28 ± 0.07 for

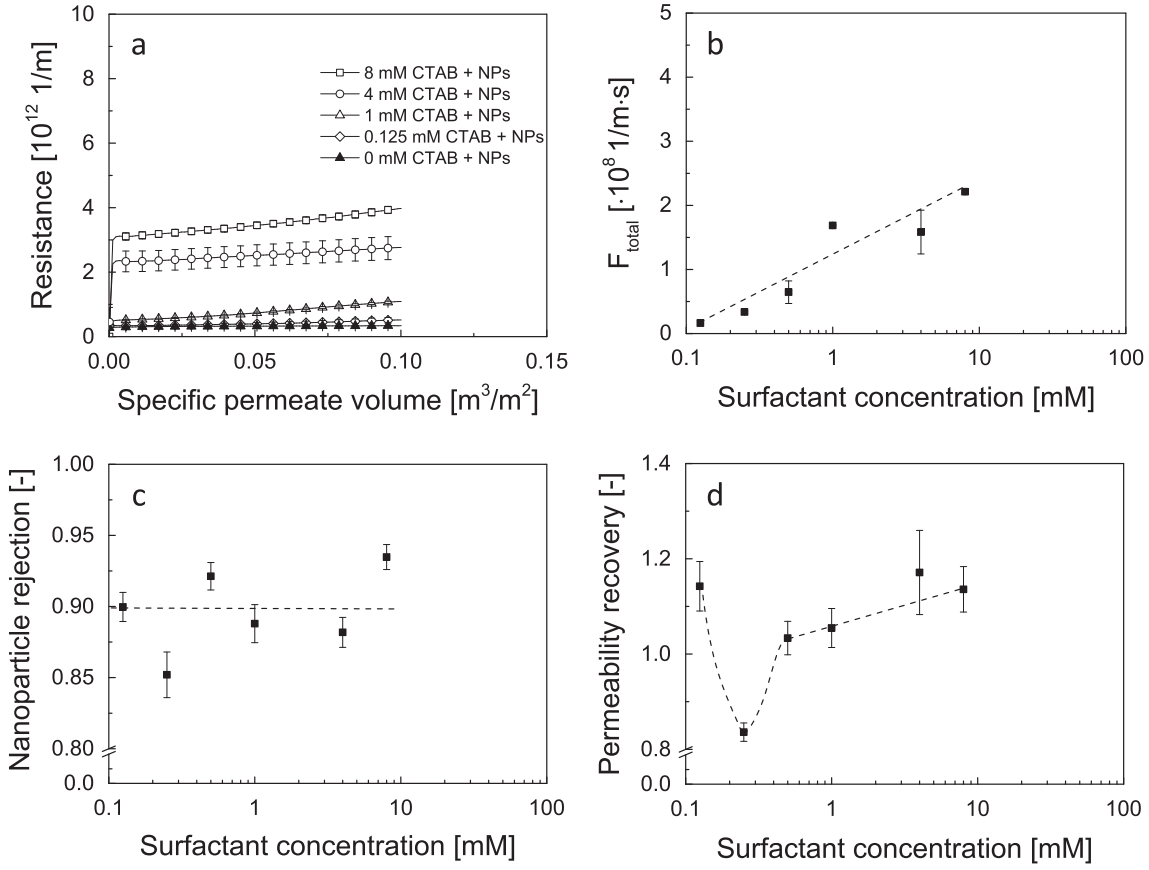

Fig. 7. (a) Resistance development as a function of permeate volume, (b) fouling rate, (c) rejection of nanoparticles and (d) permeability recovery as a function of surfactant concentration during constant flux dead-end filtration at 30 °C of 50 mg/L silica nanoparticles with cationic CTAB. Dashed lines are drawn to guide the eye.

4 mM and 8 mM, respectively. We speculate that at lower surfactant concentrations (0.125 mM–1 mM) irreversible fouling caused by the mixture of silica nanoparticles and SDS does not occur, which might be due to the moderate transmembrane pressure applied and only limited adsorption of the surfactant. At higher SDS concentrations (4 mM–8 mM), adsorption of SDS onto the membrane is facilitated and the wetting of the membrane surface is more effective. Permeability recovery is likely to be greater due to this pronounced wetting, even when nanoparticle deposition is enhanced due to the higher transmembrane pressures that need to be applied to maintain a constant permeate flux.

3.3.3. Fouling development of nanoparticles in the presence of cationic CTAB

Results obtained during the filtration of silica nanoparticles in a mixture with CTAB are summarized in Fig. 7. The observed change of the nanoparticle charge from negative to positive (see Fig. 3a) and subsequent aggregation of the nanoparticles (see Fig. 3b) does not result in a noticeably different nanoparticle filtration behavior compared to that observed for SDS. As also obtained for anionic SDS (Section 3.3.2), an increase of the cationic CTAB concentration results in more severe fouling development (see Fig. 7a). Large aggregates of nanoparticles, existing already in the bulk of the feed solution upon CTAB addition (see Fig. 3b), result in the formation of a non-uniform filtration cake, full of defects. Furthermore, an increase in the nanoparticle size results in a more open filtration cake and thus reduced the contribution of the nanoparticle deposit to the filtration resistance. Based on these observations, we suggest that the development of the resistance is dominated by the CTAB concentration in the feed solution and aggregated nanoparticles do not contribute significantly to fouling development. This hypothesis is supported by the fact that the fouling rate rises linear with the logarithm of CTAB concentration (Fig. 7b), and thus no synergic effect between nanoparticles and CTAB on fouling is observed.

In the case of CTAB, nanoparticle rejection varies from approx. 85% for 0.25 mM CTAB to 95% for 8 mM CTAB (see Fig. 7c). The data obtained for CTAB are more scattered than for SDS, with large error bars, and it is more difficult to observe a clear correlation between surfactant concentration and rejection. We can associate this lower nanoparticle rejection and its irreproducibility to the aggregation of nanoparticles in the feed solution (see Fig. 3b) and the previously mentioned non-uniform nanoparticle deposition on the membrane surface. Since aggregation is a kinetic process, it can lead to a non-uniform size distribution of the nanoparticles in the feed solution during separate filtration runs. As a result, the uniformity of the filtration cake will vary for each of the separate filtration runs. This effect is pronounced more for CTAB than for the two other surfactants. Poor control over the aggregate size can be also responsible for the poor correlation between surfactant concentration and nanoparticle rejection. Surprisingly, the nanoparticle rejection is the lowest when CTAB is present in the feed solution (compared to the other surfactants). Although intuitively one would think that the formation of nanoparticle aggregates would result in higher rejections, the aggregation of nanoparticles in the feed solution can result in a non-uniform thickness of the filtration cake and formation of isolated areas on the membrane surface that are less effectively covered by the nanoparticle deposit. Transport of some non-aggregated nanoparticles through the membrane is facilitated in such regions resulting in slightly lower nanoparticle rejections. However, to validate this

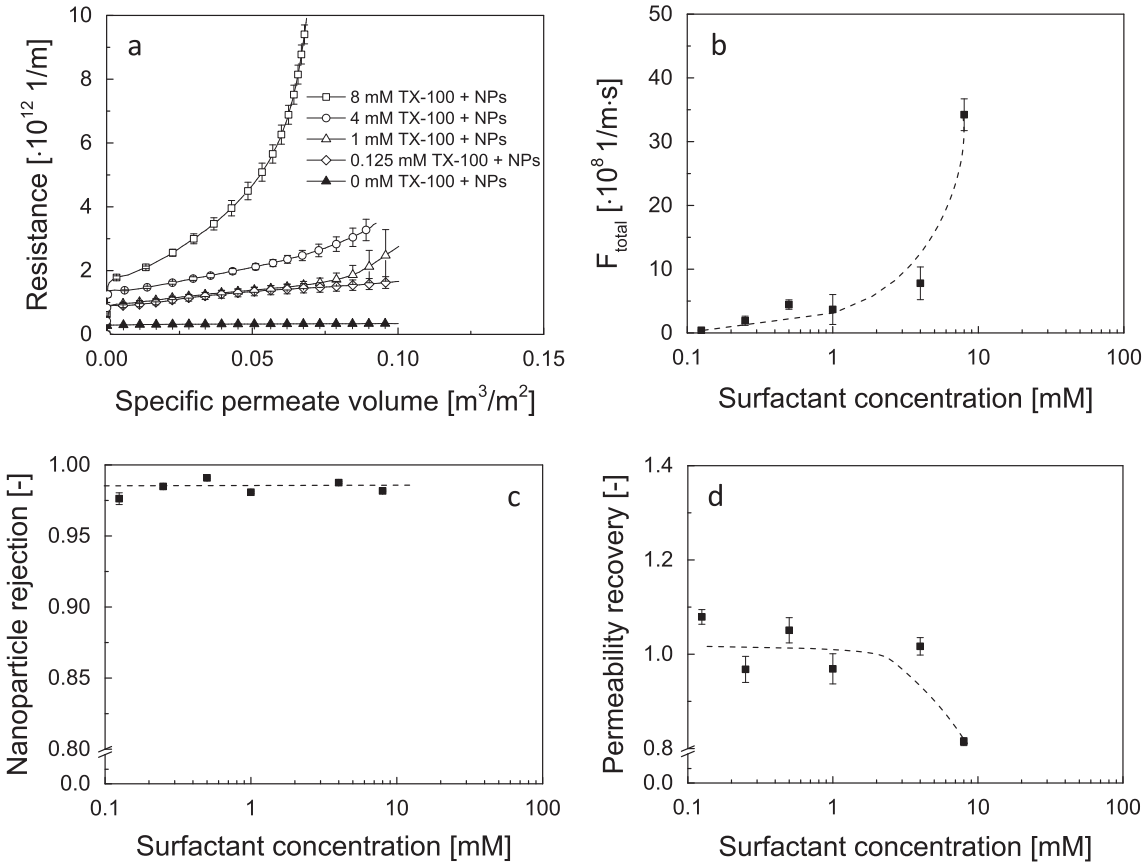

Fig. 8. (a) Resistance development as a function of permeate volume, (b) fouling rate, (c) rejection of nanoparticles and (d) permeability recovery as a function of surfactant concentration during constant flux dead-end filtration of 50 mg/L silica nanoparticles at 30 °C with non-ionic TX-100. The dashed lines are drawn only to guide the eye.

assumption additional detailed investigations on the transport phenomena of CTAB-coated silica nanoparticles in porous media need to be carried out, which is beyond the scope of this work.

The permeability recovery obtained after filtration of silica nanoparticles in a mixture with CTAB is plotted in Fig. 7d. The results obtained for cationic CTAB are similar to those obtained for anionic SDS. At the lowest investigated surfactant concentration (0.125 mM), permeability recovery was about 1.14 ± 0.05 (PR > 1) indicating reduced nanoparticle deposition and wetting of the membrane. By increasing the concentration of CTAB to 0.25 mM, the transmembrane pressure during the filtration rises and more irreversible fouling is observed since permeability recovery decreases to about 0.84 ± 0.02 (PR < 1). However, a further increase of the CTAB concentration causes improved wetting of the fibers and permeability the recovery raises again (PR > 1).

3.3.4. Fouling development of nanoparticles in the presence of non-ionic TX-100

From all three investigated surfactants, the presence of the non-ionic TX-100 in the feed solution causes the most severe fouling development, as shown in Fig. 8a. Like for the other two ionic surfactants, an increase of the TX-100 surfactant concentration also caused greater filtration resistance. Furthermore, from a concentration of 1 mM, 4 mM and 8 mM of TX-100, the resistance increases exponentially with specific permeate volume as opposite to the linear increase observed for the two other it was for other two surfactants. This severe fouling is not only a result of the higher surfactant load but it is clearly related to the less negative zeta potential of the nanoparticles in a mixture with TX-100 (Fig. 3a). Repulsive interactions between nanoparticles are weakened, and therefore a more compact and dense cake structure can be formed. As a result, the transmembrane pressure and filtration resistance increase considerably faster with specific permeate volume compared to those of SDS and CTAB, and in the extreme case, it grows exponentially. The significant contribution of TX-100 to fouling development is clearly illustrated in Fig. 8b, where the fouling rate is plotted as a function of the surfactant concentration. As shown in Fig. 8b, the fouling rate obtained during filtration of the silica nanoparticles with non-ionic TX-100 was one order of magnitude higher than those obtained for SDS (below 8 mM SDS, Fig. 6b) and CTAB (Fig. 7b), due to the more compact and dense deposit layer formed (different scales on the y-axis in Fig. 6b, 7b and 8b).

Addition of non-ionic TX-100 to silica nanoparticles does not change significantly the rejection in comparison to the bare nanoparticles. For all concentrations of TX-100 investigated, the rejection is 98–99%, as shown in Fig. 8c. The more compact structure of the filtration cake and the more severe fouling (Fig. 8a) compared to the other two surfactants, results in the highest nanoparticle rejection observed for the three cases described. Limited diffusion of nanoparticles across such a dense nanoparticle deposit contributes to a high nanoparticle rejection, which is rather independent of the surfactant concentration.

Fig. 8d shows that for non-ionic TX-100, the permeability recovery is the highest for the lowest surfactant concentration (0.125 mM). At intermediate surfactant concentrations, it is more or less constant (around 1) after which it reduces significantly at the highest surfactant concentration (8 mM) to 0.81 ± 0.01. The significantly higher transmembrane pressures used during filtration with 8 mM of TX-100 than those for all the other filtration runs and the lower repulsive interactions between the nanoparticles in the presence of TX-100 can explain the reduced permeability recovery. We think that wetting of the membrane at increased TX-100 surfactant concentration is dominated by extensive irreversible fouling, as opposed to the behavior of the anionic and cationic surfactants (Fig. 6d and 7d).

4. Conclusions

In this experimental study, we investigated the effect of three different types of commercial surfactants (CTAB, SDS and TX-100) on the fouling development during hollow fiber dead-end ultrafiltration of silica nanoparticles and tried to give insight into the mechanisms of nanoparticle rejection and fouling development.

As previously stated, the stability of the nanoparticle suspension is found to be dependent on the type of surfactant (e.g. [12]). Similarly to before published results, the most prominent aggregation of nanoparticles in the feed solution is observed after addition of CTAB, where the surface charge of the nanoparticles is inverted from negative to positive [15]. Non-ionic TX-100 neutralizes the surface charge of the silica nanoparticles causing a slight increase in the nanoparticle size [22]. Anionic SDS does not interact extensively with the negatively charged silica nanoparticles [15].

Contrary to the work of Singh and Song [18], any addition of anionic SDS to the feed solution has a synergic effect on fouling development. However, below the CMC value of SDS this synergic contribution of SDS to fouling development was limited, whereas, above the CMC, fouling develops much strongly, which might occur due to the formation of a more compact gel layer as previously reported in literature. For cationic CTAB, aggregation of the nanoparticles results in only a limited contribution of the nanoparticles to the built up of the filtration resistance and fouling development is dominated by the surfactant concentration. Addition of non-ionic TX-100 to the nanoparticle suspension indisputably reduces the repulsive interactions between the nanoparticles thus severely enhancing fouling. Furthermore, we observe that for each surfactant fouling is more pronounced at higher surfactant concentration.

Also, the nanoparticle rejection is influenced by the type of surfactant type and the concentration. In general, nanoparticle rejection increased in the order of CTAB-silica < SDS-silica < TX-100-silica. We speculate that the difference in nanoparticle rejection has its origin in the homogeneity and density of the cake layer formed. Fouling irreversibility is difficult to assess due to additional wetting phenomena of the fibers in the presence of the surfactants. In some cases this results in permeability recoveries above 1.

In general, we can conclude that surfactants play a complex role in the fouling behavior of nanoparticles as they interact with the membrane, with the nanoparticles and with other surfactant molecules. Our investigation provides some insights into the role of the surfactant on nanoparticle stability and the mechanisms responsible for fouling during filtration of mixtures containing both nanoparticles and surfactants. However, a fundamental investigation of the dynamic changes of fouling mechanisms occurring at the surface of the semipermeable membrane is necessary in order to better understand the phenomena occurring during filtration of nanoparticles with surfactants

Acknowledgement

This work is supported by NanoNextNL, a micro- and nanotechnology consortium of the Government of the Netherlands and 130 partners. We especially acknowledge Vitens N.V. for the ICP-MS measurements.

References

[1] Willems, v. d. Wildenberg, Roadmap report on nanoparticles, W&W Espana s.l., Barcelona, Spain (2005).
[2] T.E. Abbott Chalew, G.S. Ajmani, H. Huang, K.J. Schwab, Evaluating nanoparticle breakthrough during drinking water treatment, Environ. Health. Perspect. 121 (2013) 1161–1166.

[3] A.I. Schäfer, U. Schwicker, M.M. Fischer, A.G. Fane, T.D. Waite, Microfiltration of colloids and natural organic matter, J. Membr. Sci. 171 (2000) 151–172.
[4] A.S. Kim, A.E. Contreras, Q. Li, R. Yuan, Fundamental mechanisms of three-component combined fouling with experimental verification, Langmuir 25 (2009) 7815–7827.
[5] A.H. Taheri, L.N. Sim, C.T. Haur, E. Akhondi, A.G. Fane, The fouling potential of colloidal silica and humic acid and their mixtures, J. Membr. Sci. 433 (2013) 112–120.
[6] P. Aimar, P. Bacchin, Slow colloidal aggregation and membrane fouling, J. Membr. Sci. 360 (2010) 70–76.
[7] D. Jassby, S.R. Chae, Z. Hendren, M. Wiesner, Membrane filtration of fullerene nanoparticle suspensions: effects of derivatization, pressure, electrolyte species and concentration, J. Colloid Interface Sci. 346 (2010) 296–302.
[8] T. Yin, H.W. Walker, D. Chen, Q. Yang, Influence of pH and ionic strength on the deposition of silver nanoparticles on microfiltration membranes, J. Membr. Sci. 449 (2014) 9–14.
[9] Y. Chen, H. Kim, Monte Carlo simulation of pore blocking and cake formation by interfacial interactions during membrane filtration, Desalination 233 (2008) 258–266.
[10] S.T.V. Sim, A.H. Taheri, T.H. Chong, W.B. Krantz, A.G. Fane, Colloidal metastability and membrane fouling – Effects of crossflow velocity, flux, salinity and colloid concentration, J. Membr. Sci. 469 (2014) 174–187.
[11] J. Labille, J. Brant, Stability of nanoparticles in water, Nanomedicine 5 (2010) 985–998.
[12] S.Y. Moon, T. Kusunose, T. Sekino, CTAB-Assisted synthesis of size- and shape-controlled gold nanoparticles in SDS aqueous solution, Mater. Lett. 63 (2009) 2038–2040.
[13] Z. Tan, H. Abe, M. Naito, S. Ohara, Oriented growth behavior of Ag nanoparticles using SDS as a shape director, J. Colloid Interface Sci. 348 (2010) 289–292.
[14] W. Zhang, X. Qiao, J. Chen, Formation of silver nanoparticles in SDS inverse microemulsions, Mater. Chem. Phys. 109 (2008) 411–416.
[15] S. Ahualli, G.R. Iglesias, W. Wachter, M. Dulle, D. Minami, O. Glatter, Adsorption of anionic and cationic surfactants on anionic colloids: supercharging and destabilization, Langmuir 27 (2011) 9182–9192.
[16] V.L. Alexeev, P. Ilekti, J. Persello, J. Lambard, T. Gulik, B. Cabane, Dispersions of silica particles in surfactant phases, Langmuir 12 (1996) 2392–2401.
[17] G.M. Litton, T.M. Olson, Colloid deposition rates on silica bed media and artifacts related to collector surface preparation methods, Environ. Sci. Technol. 27 (1993) 185–193.
[18] G. Singh, L. Song, Influence of sodium dodecyl sulfate on colloidal fouling potential during ultrafiltration, Colloids Surf., A 281 (2006) 138–146.
[19] Y. Liu, M. Tourbin, S. Lachaize, P. Guiraud, Silica nanoparticles separation from water: Aggregation by cetyltrimethylammonium bromide (CTAB), Chemosphere 92 (2013) 681–687.
[20] Y. Gao, J. Du, T. Gu, Hemimicelle formation of cationic surfactants at the silica gel-water interface, J. Chem. Soc. Faraday Trans. I (83) (1987) 2671–2679.
[21] P. Somasundaran, D.W. Fuerstenau, Mechanisms of alkyl sulfonate adsorption at the alumina-water interface, J. Phys. Chem. A 70 (1966) 90–96.
[22] F. Giordano-Palmino, R. Denoyel, J. Rouquerol, Interfacial aggregation of a nonionic surfactant: effect on the stability of silica suspensions, J. Colloid Interface Sci. 165 (1994) 82–90.
[23] M. Prasad, R. Palepu, S.P. Moulik, Interaction between sodium dodecyl sulfate (SDS) and polyvinylpyrrolidone (PVP) investigated with forward and reverse component addition protocols employing tensiometric, conductometric, microcalorimetric, electrokinetic, and DLS techniques, Colloid Polym. Sci. 284 (2006) 871–878.
[24] S.X. Liu, J.-T. Kim, Study of adsorption kinetics of surfactants onto polyethersulfone membrane surface using QCM-D, Desalination 247 (2009) 355–361.
[25] F. Fairbrother, H. Mastin, CCCXII.-Studies in electro-endosmosis. Part I, J. Chem. Soc., Trans. 125 (1924) 2319–2330.
[26] F.P. Cuperus, D. Bargeman, C.A. Smolders, Permporometry. The determination of the size distribution of active pores in UF membranes, J. Membr. Sci. 71 (1992) 57–67.
[27] M.A. Khosa, S.S. Shah, M.F. Nazar, UV-visible spectrometric study and micellar enhanced ultrafiltration of alizarin red S dye, J. Dispersion Sci. Technol. 32 (2011) 1634–1640.
[28] W.J.C. van de Ven, K.v.t. Sant, I.G.M. Pünt, A. Zwijnenburg, A.J.B. Kemperman, W.G.J. van der Meer, et al., Hollow fiber dead-end ultrafiltration: Influence of ionic environment on filtration of alginates, J. Membr. Sci. 308 (2008) 218–229.
[29] P. van der Marel, A. Zwijnenburg, A. Kemperman, M. Wessling, H. Temmink, W. van der Meer, An improved flux-step method to determine the critical flux and the critical flux for irreversibility in a membrane bioreactor, J. Membr. Sci. 332 (2009) 24–29.
[30] G. Duplâtre, M.F. Ferreira Marques, M. da Graça Miguel, Size of sodium dodecyl sulfate micelles in aqueous solutions as studied by positron annihilation lifetime spectroscopy, J. Phys. Chem. 100 (1996) 16608–16612.
[31] M.S. Bakshi, A. Kaura, J.D. Miller, V.K. Paruchuri, Sodium dodecyl sulfate–poly (amidoamine) interactions studied by AFM imaging, conductivity, and Krafft temperature measurements, J. Colloid Interface Sci. 278 (2004) 472–477.
[32] W. Zhang, G. Li, J. Mu, Q. Shen, L. Zheng, H. Liang, et al., Effect of KBr on the micellar properties of CTAB, Chin. Sci. Bull. 45 (2000) 1854–1857.
[33] K. Eskilsson, V.V. Yaminsky, Deposition of monolayers by retraction from solution: ellipsometric study of cetyltrimethylammonium bromide adsorption at silica–air and silica–water interfaces, Langmuir 14 (1998) 2444–2450.
[34] C.C. Ruiz, J.A. Molina-Bolívar, J. Aguiar, G. MacIsaac, S. Moroze, R. Palepu, Thermodynamic and structural studies of triton X-100 micelles in ethylene glycol–water mixed solvents, Langmuir 17 (2001) 6831–6840.
[35] M. Luckey, Membrane Structural Biology: With Biochemical and Biophysical Foundations, Cambridge University Press, 2014.
[36] S. Kumar, V.K. Aswal, J. Kohlbrecher, Size-dependent interaction of silica nanoparticles with different surfactants in aqueous solution, Langmuir 28 (2012) 9288–9297.
[37] R. Atkin, V.S.J. Craig, S. Biggs, Adsorption kinetics and structural arrangements of cationic surfactants on silica surfaces, Langmuir 16 (2000) 9374–9380.
[38] S.C. Howard, V.S.J. Craig, Very slow surfactant adsorption at the solid-liquid interface is due to long lived surface aggregates, Soft Matter 5 (2009) 3061–3069.
[39] E. Tyrode, M.W. Rutland, C.D. Bain, Adsorption of CTAB on hydrophilic silica studied by linear and nonlinear optical spectroscopy, J. Am. Chem. Soc. 130 (2008) 17434–17445.
[40] E.Y. Bryleva, N.A. Vodolazkaya, N.O. McHedlov-Petrossyan, L.V. Samokhina, N. A. Matveevskaya, A.V. Tolmachev, Interfacial properties of cetyltrimethylammonium-coated SiO_2 nanoparticles in aqueous media as studied by using different indicator dyes, J. Colloid Interface Sci. 316 (2007) 712–722.
[41] P. Levitz, H. Van Damme, D. Keravis, Fluorescence decay study of the adsorption of nonionic surfactants at the solid-liquid interface. 1. Structure of the adsorption layer on a hydrophilic solid, J. Phys. Chem. 88 (1984) 2228–2235.
[42] A.-S. Jönsson, B. Jönsson, The influence of nonionic and ionic surfactants on hydrophobic and hydrophilic ultrafiltration membranes, J. Membr. Sci. 56 (1991) 49–76.
[43] J.T.F. Keurentjes, M.A.C. Stuart, D. Brinkman, C.G.P.H. Schroën, K. van 't Riet, Surfactant-induced wetting transitions: role of surface hydrophobicity and effect on oil permeability of ultrafiltration membranes, Colloids Surf. 51 (1990) 189–205.
[44] M.J. Rosa, M.N. de Pinho, Membrane surface characterisation by contact angle measurements using the immersed method, J. Membr. Sci. 131 (1997) 167–180.
[45] J. Chen, M. Zhang, F. Li, L. Qian, H. Lin, L. Yang, X. Wu, X. Zhou, Y. He, B.-Q. Liao, Membrane fouling in a membrane bioreactor: high filtration resistance of gel layer and its underlying mechanism, Water Res. 102 (2016) 82–89.
[46] M. Zhang, W. Peng, J. Chen, Y. He, L. Ding, A. Wang, H. Lin, H. Hong, Y. Zhang, H. Yu, A new insight into membrane fouling mechanism in submerged membrane bioreactor: Osmotic pressure during cake layer filtration, Water Res. 47 (2013) 2777–2786.
[47] K.W. Trzaskus, W.M. de Vos, A.J.B. Kemperman, K. Nijmeijer, Towards controlled fouling and rejection in dead-end microfiltration of nanoparticles – role of electrostatic interactions, J. Membr. Sci. 496 (2015) 174–184.
[48] G.P. Van der Beek, M.A.C. Stuart, T. Cosgrove, Polymer adsorption and desorption studies via proton NMR relaxation of the solvent, Langmuir 7 (1991) 327–334.
[49] R.M. McDonogh, A.G. Fane, C.J.D. Fell, H.-C. Flemming, The influence of polydispersity on the hydraulic behaviour of colloidal fouling layers on membranes: Perturbations on the behaviour of the "ideal" colloidal layer, Colloids Surf., A 138 (1998) 231–244.